

A representer theorem for deep kernel learning

Bastian Bohn[†]

Michael Griebel^{†‡}

Christian Rieger[†]

June 13, 2022

Abstract

In this paper we provide a representer theorem for a concatenation of (linear combinations of) kernel functions of reproducing kernel Hilbert spaces. This fundamental result serves as a first mathematical foundation for the analysis of machine learning algorithms based on compositions of functions. As a direct consequence of this new representer theorem, the corresponding infinite-dimensional minimization problems can be recast into (nonlinear) finite-dimensional minimization problems, which can be tackled with nonlinear optimization algorithms. In this context, we show how concatenated machine learning problems can be reformulated as neural networks and how our representer theorem applies to a broad class of state-of-the-art deep learning methods. We use our results to establish deep learning algorithms based on the composition of functions from reproducing kernel Hilbert spaces.

1 Introduction

The interpolation or regression of given function values is one of the main tasks in modern data mining and machine learning applications. Due to the famous representer theorem for empirical risk minimization in reproducing kernel Hilbert spaces (RKHS), see e.g. [12, 19], various algorithms based on finite linear combinations of kernel translates have gained much popularity in the last decades, e.g. support vector machines (SVMs) and Tikhonov-regularized least-squares in RKHS. In general, these methods work very well if it is known that the underlying problem fits the chosen reproducing kernel space H , e.g. if the given input values stem from a function $g \in H$. However, if H contains only smooth functions for instance and g has a kink or a jump, the interpolant or regressor, respectively, in H might not represent a good approximation to the true function g . If it is not known how to choose an appropriate kernel K of H a priori, one usually relies on so-called multiple kernel learning (MKL) algorithms, which try to determine the optimal kernel adaptively, see e.g. [2]. While most of these methods allow to learn a suitable kernel by simply constructing a linear or convex combination of a given set of input kernels, they still do not achieve considerably better results than standard a-priori kernel choices for many applications, see [10].

In recent years, promising new variants of kernel learning methods, namely deep kernel learning and multilayer-MKL (MLMKL) algorithms have been developed. Here, motivated by multilayer feed-forward neural networks, a kernel function is concatenated with one or more nonlinear functions in order to achieve a highly flexible new kernel function, see e.g. [5, 7, 17, 20, 22, 23]. These methods have proven to be very successful in regression and classification tasks. While first steps towards creating a mathematical framework to analyze deep neural networks - especially for image classification tasks - have been made in e.g. [13, 14, 16], deep approximation theory for kernel based approaches is still missing at large. Moreover, the underlying

[†]Institute for Numerical Simulation, University of Bonn, Wegelerstr. 6, 53115 Bonn, Germany.

[‡]Fraunhofer Institute for Algorithms and Scientific Computing SCAI, Schloss Birlinghoven, 53754 Sankt Augustin, Germany.

The authors were partially supported by the Sonderforschungsbereich 1060 *The Mathematics of Emergent Effects* funded by the Deutsche Forschungsgemeinschaft.

nonlinear minimization problem is usually tackled by simple gradient descent and heuristic backpropagation algorithms without a thorough theoretical analysis of its properties.

In this paper, we consider the problem of optimal concatenated approximation in reproducing kernel Hilbert spaces, which will directly lead to a variant of a multi-layer kernel learning problem. For this class, we will be able to prove a representer theorem, which allows us to reduce the nonlinear, potentially infinite-dimensional optimization problem to a finite-dimensional one. Consequently, standard nonlinear optimization techniques can be used to tackle this problem. At least to our knowledge, this is the first derivation of a representer theorem for concatenated function approximation in the literature. It is also valid for certain types of hidden layer neural networks and deep SVMs. This new representer theorem will be the foundation for a rigorous analysis of the associated minimization problems and for building appropriate finite-dimensional algorithms to tackle them.

The rest of this paper is organized as follows: We briefly review the interpolation and the regression problem in an (possibly infinite-dimensional) RKHS and discuss how the representer theorem allows to recast these problems into finite-dimensional linear equation systems in section 2. In section 3, we introduce the optimal concatenated approximation problem for arbitrary loss functions and regularizers. We derive a representer theorem for this problem in the multi-layer case and show how it can be applied to derive algorithms for interpolation and least-squares regression in the two-layer case. Furthermore, we discuss its relation to deep learning and multilayer multiple kernel learning methods. Section 4 illustrates how the concatenated interpolation and regression algorithms perform in numerical experiments in contrast to the (standard) single-layer variant. Finally, we conclude with a summary and an outlook in section 5.

2 Interpolation and regression in reproducing kernel Hilbert spaces

In this section we shortly review interpolation and least-squares regression problems, respectively, in an RKHS. To this end, we consider the standard representer theorem and show how it helps to find an interpolant/regressor.

2.1 Interpolation

Let $\Omega \subset \mathbb{R}^d$ be an open domain and let the (pairwise disjoint) data points $X := \{\mathbf{x}_1, \dots, \mathbf{x}_N\} \subset \Omega$ and the values $Y := \{y_1, \dots, y_N\} \subset \mathbb{R}$ be given. Let furthermore $H := H(\Omega, \mathbb{R})$ be a reproducing kernel Hilbert space of real-valued functions on Ω . The minimal norm interpolant is

$$f_{X,Y}^* := \arg \min_{f \in H} \|f\|_H \quad \text{such that} \quad f(\mathbf{x}_i) = y_i \quad \forall i = 1, \dots, N. \quad (1)$$

The classical representer theorem, see e.g. [19] for scalar-valued functions and [15] for vector-valued functions, now states that $f_{X,Y}^*$ can be written as a *finite* linear combination of kernel evaluations in the data, namely

$$f_{X,Y}^*(\mathbf{x}) = \sum_{i=1}^N \alpha_i^* K(\mathbf{x}_i, \mathbf{x}), \quad (2)$$

where $K : \Omega \times \Omega \rightarrow \mathbb{R}$ denotes the reproducing kernel of H and $\alpha_i^* \in \mathbb{R}, i = 1, \dots, N$ are the corresponding coefficients. For details on RKHS, see [1]. Therefore, the solution to the possibly infinite-dimensional optimization problem (1) resides in the N -dimensional span of the functions $K(\mathbf{x}_i, \cdot), i = 1, \dots, N$. To compute the coefficients, we simply have to solve the system

$$\mathbf{M}_{X,X} \boldsymbol{\alpha}^* = \mathbf{y} \quad (3)$$

of linear equations with

$$\mathbf{M}_{X,X} := \begin{pmatrix} K(\mathbf{x}_1, \mathbf{x}_1) & \dots & K(\mathbf{x}_1, \mathbf{x}_N) \\ \vdots & \ddots & \vdots \\ K(\mathbf{x}_N, \mathbf{x}_1) & \dots & K(\mathbf{x}_N, \mathbf{x}_N) \end{pmatrix}, \quad \boldsymbol{\alpha}^* := \begin{pmatrix} \alpha_1^* \\ \vdots \\ \alpha_N^* \end{pmatrix} \quad \text{and} \quad \mathbf{y} := \begin{pmatrix} y_1 \\ \vdots \\ y_N \end{pmatrix}. \quad (4)$$

Note that this $N \times N$ system admits a unique solution if the kernel K is strictly positive definite. For example, for Sobolev kernels it can be shown that the condition number of the system matrix $\mathbf{M}_{X,X}$ only grows moderately with the size N , see [8]. Moreover, for infinitely smooth kernel functions (e.g. Gaussian kernels or multiquadrics) it can be necessary to perform an appropriate basis change before solving the above equation system, see e.g. [21].

2.2 Least-squares regression

In real-world applications, the values $y_i, i = 1, \dots, N$ are usually not exactly given, but are perturbed by some noise term. Therefore, a direct interpolation might no longer be appropriate. In this case, one considers the corresponding regularized least-squares regression problem

$$f_{X,Y}^\lambda := \arg \min_{f \in H} \lambda \|f\|_H^2 + \sum_{j=1}^N |f(\mathbf{x}_j) - y_j|^2, \quad (5)$$

where the side condition in (1) is substituted by a penalty term. Here, the Lagrange multiplier λ weights the importance of the norm minimization against the function evaluation error. Again, the representer theorem [15, 19] tells us that $f_{X,Y}^\lambda$ is of the form (2), i.e.

$$f_{X,Y}^\lambda(\mathbf{x}) = \sum_{i=1}^N \alpha_i^\lambda K(\mathbf{x}_i, \mathbf{x}).$$

This time the coefficients $\alpha_i^\lambda, i = 1, \dots, N$ are determined by

$$(\mathbf{M}_{X,X} + \lambda \mathbf{I}) \boldsymbol{\alpha}^\lambda = \mathbf{y}, \quad (6)$$

where \mathbf{I} denotes the $N \times N$ identity matrix. The size of the Lagrange parameter $\lambda > 0$ now also influences the condition number of the system matrix, i.e. the larger λ is, the smaller the condition number becomes.

3 Interpolation and regression with compositions of reproducing kernel Hilbert spaces

As already mentioned in the introduction, the standard interpolation and regression algorithms in RKHS work well if the samples y_i are (perturbed) evaluations of a function $g \in H$, where the reproducing kernel space H is known in the first place. However, if the appropriate RKHS H is unknown, it is advisable to resort to multiple kernel learning methods or multi-layer multiple kernel learning methods.

We now explain this aspect in more detail and, to this end, motivate a first two-dimensional, two-layer approach with an example: Let the kernel K of H be a tensor-product of two univariate Matern Sobolev kernels of order one on \mathbb{R} , see section 4 for a definition of this kernel. The corresponding function space H is often also called Sobolev space of ‘‘mixed smoothness’’ of order one and it is of special importance for e.g. sparse grid discretizations, see [4]. Let us consider the continuous function $g_1(x, y) := (0.1 + |x|)^{-1}$, which has a kink, which is perpendicular to the x -axis. It can easily be shown that $g_1 \in H$ and, therefore, the interpolant of g_1 by a function from H resembles a good approximation to g_1 , see Figure 1(a). If we now

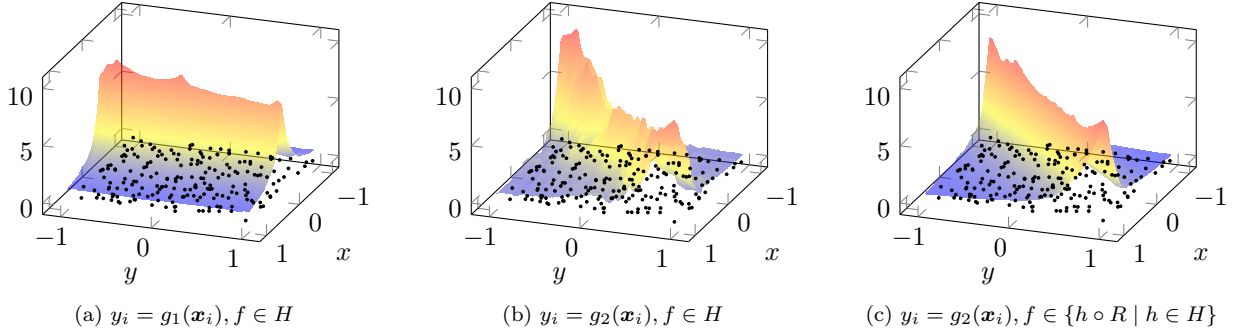


Figure 1: Solutions to (1) in the two-variate tensor-product Matern-kernel Sobolev space H of order one, see also [9], with 200 uniform samples $\mathbf{x}_i, i = 1, \dots, 200$ (marked in black). (a) depicts the solution $f \in H$ for values y_i sampled from g_1 , whereas (b) shows the optimal solution for y_i sampled from g_2 . (c) presents the best interpolant of type $f \circ R$, where $f \in H$ and R is a rotation by 45° for y_i sampled from g_2 .

look at $g_2(x, y) := (0.1 + |x - y|)^{-1}$, which has a kink along the diagonal with $x = y$, then $g_2 \notin H$. Therefore, the interpolant of g_2 by a function in H is a rather bad approximation to g_2 . This can be seen in Figure 1(b). However, if we let R^{-1} be a rotation by 45° , then $g_2 \circ R^{-1} \in H$ would have an axis-aligned kink like g_1 . To use this fact when interpolating g_2 , we can simply look for the best interpolant in $\{f \circ R \mid f \in H\}$ in (1) instead of $f \in H$. This example is illustrated in Figure 1(c). As we see, the interpolant in Figure 1(c) is a much better representative for g_2 than the one in Figure 1(b). This example illustrates that, already in the very simple case of employing a concatenation with a rotation, a two- or even multi-layer approach can be a good choice to overcome the restrictions of a standard kernel learning algorithm.

Now, instead of just considering one layer of simple rotations as in the above example, we go to a fully flexible multi-layer kernel learning approach, where we allow arbitrary functions from reproducing kernel Hilbert spaces in each layer. This approach allows to successfully deal with a much broader class of interpolation and regression problems, see also [17, 23]. To this end, we consider *concatenated* machine learning problems. We introduce a new representer theorem for the case of multiple concatenations of functions from RKHS, which allows us to derive the related, finite-dimensional, nonlinear optimization problem.

3.1 A general representer theorem for concatenated kernel learning

In this section, we show how a *concatenated representer theorem* can be derived for a very general class of problem types and an arbitrary number $L \in \mathbb{N}$ of concatenations. For more details on vector-valued reproducing kernel Hilbert spaces, we refer the reader to [15].

Theorem 1. *Let $\mathcal{H}_1, \dots, \mathcal{H}_L$ be reproducing kernel Hilbert spaces of functions with finite-dimensional domains D_l and ranges $R_l \subseteq \mathbb{R}^{d_l}$ with $d_l \in \mathbb{N}$ for $l = 1, \dots, L$ such that $R_l \subseteq D_{l-1}$ for $l = 2, \dots, L$, $D_L = \Omega$ and $R_1 \subseteq \mathbb{R}$. Let furthermore $\mathcal{L} : (\mathbb{R}^2)^N \rightarrow [0, \infty]$ be an arbitrary loss function and let $\Theta_1, \dots, \Theta_L : [0, \infty) \rightarrow [0, \infty)$ be strictly monotonically increasing functions. Then, a set of minimizers $(f_l)_{l=1}^L$ with $f_l \in \mathcal{H}_l$ of*

$$J(f_1, \dots, f_L) := \mathcal{L}((y_1, f_1 \circ \dots \circ f_L(\mathbf{x}_1)), \dots, (y_N, f_1 \circ \dots \circ f_L(\mathbf{x}_N))) + \sum_{l=1}^L \Theta_l(\|f_l\|_{\mathcal{H}_l}^2) \quad (7)$$

fulfills $f_l \in \tilde{V}_l \subset \mathcal{H}_l$ for all $l = 1, \dots, L$ with

$$\tilde{V}_l = \text{span}\{K_l(f_{l+1} \circ \dots \circ f_L(\mathbf{x}_i), \cdot) \mathbf{e}_{k_l} \mid i = 1, \dots, N \text{ and } k_l = 1, \dots, d_l\},$$

where K_l denotes the reproducing kernel of \mathcal{H}_l and $\mathbf{e}_{k_l} \in \mathbb{R}^{d_l}$ is the k_l -th unit vector.

Proof. We denote by $\Pi_{\tilde{V}_l}$ and $\Pi_{\tilde{V}_l^\perp}$ the projector onto \tilde{V}_l and its orthogonal complement in \mathcal{H}_l , respectively, for $l = 1, \dots, L$. First, we note that

$$\begin{aligned} f_l \circ f_{l+1} \circ \dots \circ f_L(\mathbf{x}_i) &= \sum_{k=1}^{d_l} \left(\Pi_{\tilde{V}_l}(f_l) + \Pi_{\tilde{V}_l^\perp}(f_l), K_l(f_{l+1} \circ \dots \circ f_L(\mathbf{x}_i), \cdot) \mathbf{e}_k \right)_{\mathcal{H}_l} \cdot \mathbf{e}_k \\ &= \sum_{k=1}^{d_l} \left(\Pi_{\tilde{V}_l}(f_l), K_l(f_{l+1} \circ \dots \circ f_L(\mathbf{x}_i), \cdot) \mathbf{e}_k \right)_{\mathcal{H}_l} \cdot \mathbf{e}_k \\ &= \sum_{k=1}^{d_l} \left(\mathbf{e}_k^T \Pi_{\tilde{V}_l}(f_l) (f_{l+1} \circ \dots \circ f_L(\mathbf{x}_i)) \right) \cdot \mathbf{e}_k \\ &= \Pi_{\tilde{V}_l}(f_l) (f_{l+1} \circ \dots \circ f_L(\mathbf{x}_i)) \end{aligned}$$

for all $i = 1, \dots, N$ and $l = 1, \dots, L$. Since this holds for each function in the chain, we can iterate this process to obtain

$$f_l \circ f_{l+1} \circ \dots \circ f_L(\mathbf{x}_i) = \Pi_{\tilde{V}_l}(f_l) \circ \Pi_{\tilde{V}_{l+1}}(f_{l+1}) \circ \dots \circ \Pi_{\tilde{V}_L}(f_L)(\mathbf{x}_i) \quad (8)$$

for each $l = 1, \dots, L$. Therefore, we have

$$\begin{aligned} J(f_1, \dots, f_L) &= \mathcal{L} \left((y_1, \Pi_{\tilde{V}_1}(f_1) \circ \dots \circ \Pi_{\tilde{V}_L}(f_L)(\mathbf{x}_1)), \dots, (y_N, \Pi_{\tilde{V}_1}(f_1) \circ \dots \circ \Pi_{\tilde{V}_L}(f_L)(\mathbf{x}_N)) \right) \\ &+ \sum_{l=1}^L \Theta_l \left(\|\Pi_{\tilde{V}_l}(f_l)\|_{\mathcal{H}_l}^2 + \|\Pi_{\tilde{V}_l^\perp}(f_l)\|_{\mathcal{H}_l}^2 \right) \geq J(\Pi_{\tilde{V}_1}(f_1), \dots, \Pi_{\tilde{V}_L}(f_L)) \end{aligned}$$

and equality only holds if $f_l \in \tilde{V}_l$ for each $l = 1, \dots, L$ because of the strict monotonicity of each Θ_l . This completes the proof. \square

Note that, because of (8), we could even state a more general version of Theorem 1 where the loss function \mathcal{L} not only depends on the point evaluations $f_1 \circ \dots \circ f_L(\mathbf{x}_i)$ for $i = 1, \dots, N$, but also on the intermediate values $f_l \circ \dots \circ f_L(\mathbf{x}_i)$ for any $l = 2, \dots, L$. However, for the sake of readability, we cope with (7). Theorem 1 now states that

$$(f_1, \dots, f_L) = \arg \min_{\substack{\bar{f}_l \in \mathcal{H}_l \\ l=1, \dots, L}} J(\bar{f}_1, \dots, \bar{f}_L) = \arg \min_{\substack{\bar{f}_l \in \tilde{V}_l \\ l=1, \dots, L}} J(\bar{f}_1, \dots, \bar{f}_L) \quad (9)$$

with J from (7). This means that the (possibly) infinite-dimensional optimization problem

$$\arg \min_{\substack{\bar{f}_l \in \mathcal{H}_l \\ l=1, \dots, L}} J(\bar{f}_1, \dots, \bar{f}_L)$$

can be recast into the finite-dimensional optimization problem

$$\arg \min_{\substack{\bar{f}_l \in \tilde{V}_l \\ l=1, \dots, L}} J(\bar{f}_1, \dots, \bar{f}_L).$$

In this way, our representer theorem is a direct extension of the classical representer theorem, see section 2 and [19], to concatenated functions. We obtain that the solution to (9) is given by a linear combination of at most N basis functions in each layer. Therefore, the overall number of degrees of freedom in the underlying optimization problem (9) is given by

$$\# \text{dof} = \sum_{l=1}^L \dim(\tilde{V}_l) = \sum_{l=1}^L N \cdot d_l = N \cdot \left(1 + \sum_{l=2}^L d_l \right).$$

According to Theorem 1, we can write f_1 as

$$f_1(\cdot) = \sum_{j=1}^N \alpha_j K_1(f_2 \circ \dots \circ f_L(\mathbf{x}_j), \cdot)$$

for some coefficients $\alpha_j \in \mathbb{R}$. Therefore, the concatenated function $h(\cdot) = f_1 \circ \dots \circ f_L(\cdot)$, which we are interested in, can be expressed as

$$h(\cdot) = \sum_{j=1}^N \alpha_j \mathcal{K}^L(\mathbf{x}_j, \cdot)$$

with the deep kernel

$$\mathcal{K}^L(\mathbf{x}, \mathbf{y}) = K_1(f_2 \circ \dots \circ f_L(\mathbf{x}_j), f_2 \circ \dots \circ f_L(\cdot)). \quad (10)$$

Due to the definition of \tilde{V}_l for $l = 1, \dots, L$, the corresponding f_l is defined recursively and it is, thus, not possible to write down a closed formula for \mathcal{K}^L for general L . To illustrate the structure of the deep kernel, we therefore consider a two-layer example with $L = 2$ in the following. In this case, we obtain $\tilde{V}_2 = \text{span}\{K_2(\mathbf{x}_i, \cdot)\mathbf{e}_{k_2} \mid i = 1, \dots, N \text{ and } k_2 = 1, \dots, d_2\}$. From Theorem 1, we know that

$$f_2(\cdot) = \sum_{i=1}^N \sum_{k_2=1}^{d_2} c_{i,k_2} K_2(\mathbf{x}_i, \cdot)\mathbf{e}_{k_2}$$

for certain coefficients $c_{i,k_2} \in \mathbb{R}$. Furthermore, we have that $f_1 \in \tilde{V}_1 = \text{span}\{K_1(f_2(\mathbf{x}_i), \cdot) \mid i = 1, \dots, N\}$ and thus

$$f_1(\cdot) = \sum_{j=1}^N \alpha_j K_1\left(\sum_{i=1}^N \sum_{k_2=1}^{d_2} c_{i,k_2} K_2(\mathbf{x}_i, \mathbf{x}_j)\mathbf{e}_{k_2}, \cdot\right).$$

The concatenated function is then given by $h(\cdot) := f_1 \circ f_2(\cdot) = \sum_{j=1}^N \alpha_j \mathcal{K}^2(\mathbf{x}_j, \cdot)$ with the composition kernel

$$\mathcal{K}^2(\mathbf{x}, \mathbf{y}) = K_1\left(\sum_{i=1}^N \sum_{k_2=1}^{d_2} c_{i,k_2} K_2(\mathbf{x}_i, \mathbf{x})\mathbf{e}_{k_2}, \sum_{i=1}^N \sum_{k_2=1}^{d_2} c_{i,k_2} K_2(\mathbf{x}_i, \mathbf{y})\mathbf{e}_{k_2}\right). \quad (11)$$

Therefore, instead of considering the infinite-dimensional optimization problem of finding $f_1 \in \mathcal{H}_1$ and $f_2 \in \mathcal{H}_2$ that minimize

$$J(f_1, f_2) = \mathcal{L}((y_1, f_1(f_2(\mathbf{x}_1))), \dots, (y_N, f_1(f_2(\mathbf{x}_N)))) + \Theta_1(\|f_1\|_{\mathcal{H}_1}^2) + \Theta_2(\|f_2\|_{\mathcal{H}_2}^2),$$

we can restrict ourselves to finding the $N + N \cdot d_2$ coefficients α_j, c_{i,k_2} for $i, j = 1, \dots, N$ and $k_2 = 1, \dots, d_2$. Note at this point that the problem of finding these coefficients is highly nonlinear and becomes more complicated for a larger number of layers L . While the corresponding problem of optimizing the outermost coefficients, i.e. α_j for $j = 1, \dots, N$ in our example, is still convex if the loss \mathcal{L} and the penalty terms Θ_1, Θ_2 are convex, the optimization of the inner coefficients, i.e. c_{i,k_2} for $i = 1, \dots, N$ and $k_2 = 1, \dots, d_2$, is usually not convex anymore and can have many local minima. Here, finding a global minimum is problematic because standard (iterative) optimization methods strongly depend on the chosen initial value and usually just deliver some local minimum.

If the optimization functional J is smooth, one can rely on a Newton-type minimizer such as BFGS to solve the underlying optimization problem. However, if one deals with nonsmooth loss functionals or penalty terms, one should resort to specifically designed stochastic gradient algorithms which fit the problem at hand, see e.g. [18].

It remains to note that our representer theorem covers much more than just interpolation or least-squares regression algorithms. In the same fashion as the standard representer theorem in [19], it can directly be

applied to more involved settings such as regression with a concatenation of support vector machines for instance. To this end, just choose \mathcal{L} to be the ε -insensitive loss function and $\Theta_1(x) = \dots = \Theta_L(x) = x$. Furthermore, the choice of the additive penalties $\Theta_1, \dots, \Theta_L$ in (7) is rather arbitrary and one could think of more complex interactions between the penalties for each function $f_l, l = 1, \dots, L$ as long as the arguments in the proof of Theorem 1 remain valid.

3.2 Relation to neural networks and deep learning

In this section, we discuss the relation of our representer theorem to two of the most common approaches in deep learning with kernels, namely multilayer multiple kernel learning (MLMKL) and deep kernel networks (DKN), see e.g. [5, 7, 17, 20, 22, 23]. For reasons of simplicity, we restrict ourselves to the two-layer case $L = 2$ here.

3.2.1 Relation to hidden layer neural networks

Let us first illustrate how our approach can be encoded as a hidden layer feed-forward neural network. For more details on artificial neural networks and deep learning, we refer the reader to [11]. As mentioned in the two-layer case above, we are aiming to find a function $h(\cdot) = f_1 \circ f_2(\cdot) = \sum_{j=1}^N \alpha_j \mathcal{K}^2(\mathbf{x}_j, \cdot)$ with $f_1 \in \mathcal{H}_1$ and $f_2 \in \mathcal{H}_2$ and associated K_1 and K_2 , respectively, where the deep kernel \mathcal{K}^2 is given by (11).

The construction of h can be easily encoded as a feed-forward neural network with hidden layer if K_1 is a radial basis function (RBF) kernel for instance¹. We illustrate² the case $d_2 = 1$ with an RBF kernel $K_1(z_1, z_2) = a(|z_1 - z_2|)$ for some function $a: \mathbb{R} \rightarrow \mathbb{R}$ in Figure 2. The first layer is split into the input layer with values $K_2(\mathbf{x}_i, \mathbf{x})$ for $i = 1, \dots, N$ and an artificial “always on” layer with neuron-clusters that supply the constant values $K_2(\mathbf{x}_i, \mathbf{x}_j)$ with weights $-c_j$ for $i, j = 1, \dots, N$. Note that the i -th cluster $K_2(\mathbf{x}_i, \mathbf{x}_j)$ of the “always on” layer is only connected to the i -th neuron of the hidden layer. Note furthermore that the inputs $K_2(\mathbf{x}_i, \mathbf{x})$ can also easily be computed by a neural network with fixed weights if K_2 is a radial basis kernel. If we consider a “deeper” concatenation, we would need a deeper neural network with additional layers, i.e. for $f_1 \circ \dots \circ f_L$, we need $L - 1$ hidden layers.

3.2.2 Relation to multilayer multiple kernel learning

The common idea in MLMKL methods is to learn a kernel \tilde{K} , which consists of a chain of linear combinations of functions and an inner kernel, e.g.

$$\tilde{K}(\mathbf{x}, \mathbf{y}) = \sum_{\ell=1}^{n_1} \nu_{1,\ell} k_{1,\ell} \left(\sum_{i=1}^{n_2} \nu_{2,i} K_{2,i}(\mathbf{x}, \mathbf{y}) \right)$$

in the two-layer case, where $k_{1,\ell}$ are real-valued functions for $\ell = 1, \dots, n_1$ and $K_{2,i}$ are different scalar-valued kernels for $i = 1, \dots, n_2$. Note that the functions $k_{1,\ell}$ are chosen such that \tilde{K} is still a kernel. The specific MLMKL algorithm then aims to find the optimal values for the coefficients $\nu_{1,\ell}, \nu_{2,i}$ in order to determine the best \tilde{K} for a regression of the given data X and Y with e.g. a support vector regression algorithm. Note that the kernels and the k -functions are usually chosen heuristically, e.g. as polynomials, Gaussians, sigmoidals, etc., see [17, 23].

¹For many other types of kernels, e.g. tensor products of RBF kernels, one can still construct a more complex Sigma-Pi neural network for the computation of the output values.

²Note that we only choose $d_2 = 1$ for illustrative reasons. For $d_2 > 1$, a neural network can be built analogously with an additional hidden layer to compute the norm of the difference of d_2 -dimensional vectors. However, this additional layer, which just computes $\|\mathbf{x} - \mathbf{y}\|_2$ for given \mathbf{x} and \mathbf{y} , has fixed weights and does not play any role for the optimization of the neural network.

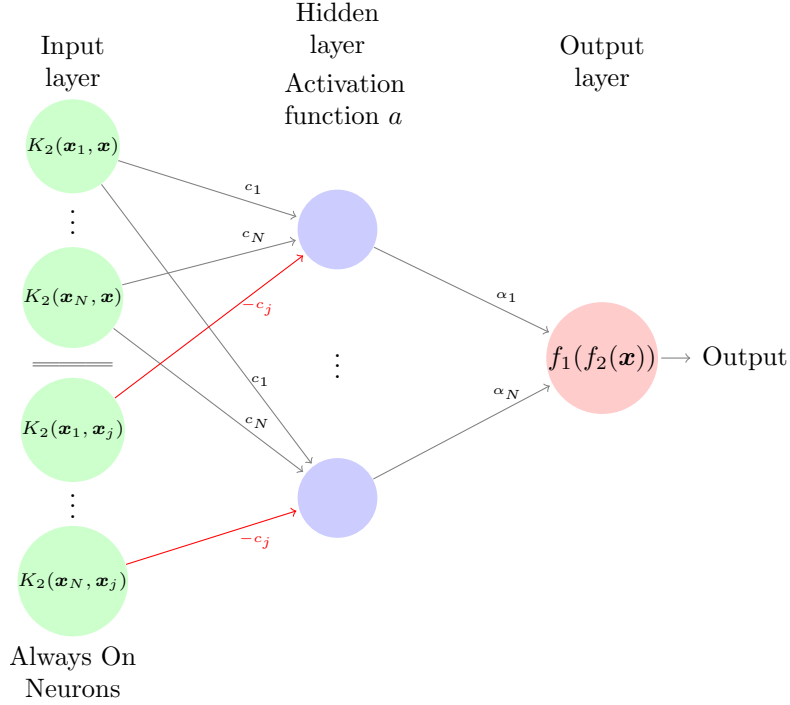


Figure 2: A hidden layer, feed-forward neural network to simulate the concatenation of two functions f_1 and f_2 from reproducing kernel Hilbert spaces. For reasons of readability, we choose $d_2 = 1$ and write $c_i := c_{i,1}$. The outer kernel is $K_1(z_1, z_2) = a(|z_1 - z_2|)$. Note that the i -th artificial “always on” neuron-cluster in the lower half of the first layer is written as $K_2(\mathbf{x}_i, \mathbf{x}_j)$, which stands for N single neurons with values $K_2(\mathbf{x}_i, \mathbf{x}_1), \dots, K_2(\mathbf{x}_i, \mathbf{x}_N)$. The cluster $K_2(\mathbf{x}_i, \mathbf{x}_j)$ is only connected to the i -th neuron of the hidden layer with weights $-c_j$ (red lines). This means that the value $\sum_{j=1}^N -c_j K_2(\mathbf{x}_i, \mathbf{x}_j)$ is forwarded to the i -th neuron of the hidden layer.

To apply our result to the two-layer MKL method above, let us consider the case $n_1 = 1$ and $n_2 = N$. We set $\nu_{1,1} = 1$ without loss of generality. We let the outer function $k_{1,1}(z) = a(|z|)$ be the radial basis function used for the outer kernel (i.e. middle layer) in Figure 2. Furthermore, we set

$$K_{2,i}(\mathbf{x}, \mathbf{y}) := K_2(\mathbf{x}_i, \mathbf{x}) - K_2(\mathbf{x}_i, \mathbf{y}).$$

Note that the $K_{2,i}$ are no longer kernels anymore in this setting. However, they are now directly connected to our concatenated function learning approach since

$$\begin{aligned} \tilde{K}(\mathbf{x}, \mathbf{y}) &= k_{1,1} \left(\sum_{i=1}^N \nu_{2,i} K_{2,i}(\mathbf{x}, \mathbf{y}) \right) = a \left(\left| \sum_{i=1}^N \nu_{2,i} K_2(\mathbf{x}_i, \mathbf{x}) - \sum_{i=1}^N \nu_{2,i} K_2(\mathbf{x}_i, \mathbf{y}) \right| \right) \\ &= K_1 \left(\sum_{i=1}^N \nu_{2,i} K_2(\mathbf{x}_i, \mathbf{x}), \sum_{i=1}^N \nu_{2,i} K_2(\mathbf{x}_i, \mathbf{y}) \right) = \mathcal{K}^2(\mathbf{x}, \mathbf{y}) \end{aligned}$$

from (11) with $c_i = \nu_{2,i}$ and the kernels K_1 and K_2 used in Figure 2. Altogether, we thus see that an MLMKL algorithm with these parameters already determines the optimal solution (provided that the right hand side of (9) is solved exactly) among all functions of type $h = f_1 \circ f_2$ with $f_1 \in \mathcal{H}_1$ and $f_2 \in \mathcal{H}_2$

according to Theorem 1. This way, our representer theorem for concatenated functions directly applies to a special case of MLMKL networks. Note however that a generalization of our arguments to more layers, i.e. $L > 2$, is not straightforward for MLMKL.

3.2.3 Relation to deep kernel learning approaches

The class of DKN methods consists of algorithms which build a kernel by nonlinearly transforming the input vectors before applying an outer kernel function. This is in contrast to the MLMKL approach, where only the innermost function is a two-variate kernel and its evaluations are modified by some nonlinear outer functions. The models in this class range from simple feature map powers for some function Ψ , i.e.

$$\tilde{K}(x, y) = \underbrace{\Psi \circ \dots \circ \Psi}_{L-1 \text{ times}}(\mathbf{x}) \cdot \underbrace{\Psi \circ \dots \circ \Psi}_{L-1 \text{ times}}(\mathbf{y}),$$

see [5], to more general variants like

$$\tilde{K}(x, y) = K(f_2 \circ \dots \circ f_L(\mathbf{x}), f_2 \circ \dots \circ f_L(\mathbf{y}))$$

with nonlinear functions f_2, \dots, f_L , see [22]. If we assume that $f_l \in \mathcal{H}_l$ for $l = 2, \dots, L$ stem from reproducing kernel Hilbert spaces with associated kernels K_l , we can apply Theorem 1 to this approach and obtain that each f_l can be written as a finite linear combination of evaluations of the kernel K_l . Thus, we can directly apply our representer theorem for L -layer DKN algorithms.

3.3 The two-layer interpolation problem

We now have a more detailed look at the interpolation problem for $L = 2$. We slightly adapt our notation to this special case to obtain a direct relation to the single-layer interpolation problem from section 2. To this end, let $D := d_2$ and consider the domain $\Phi := D_1 \subseteq \mathbb{R}^D$ together with the two function spaces

$$\begin{aligned} H(\Phi, \mathbb{R}) &:= \mathcal{H}_1 \subset C(\Phi) := \{f : \Phi \rightarrow \mathbb{R} \mid f \text{ continuous}\} && \text{-- “outer” space,} \\ \mathbf{H}(\Omega, \Phi) &:= \mathcal{H}_2 \subset \left\{ \mathbf{g} = (g_1, \dots, g_D)^T : \Omega \rightarrow \Phi \mid \mathbf{g} \text{ continuous} \right\} && \text{-- “inner” space.} \end{aligned}$$

Both spaces are supposed to be reproducing kernel Hilbert spaces, i.e. there is an (outer) kernel $K := K_1 : \Phi \times \Phi \rightarrow \mathbb{R}$ for $H(\Phi, \mathbb{R})$ such that

$$\begin{aligned} K(\mathbf{x}, \cdot) &\in H(\Phi, \mathbb{R}) && \text{for all } \mathbf{x} \in \Omega, \\ f(\mathbf{x}) &= (f, K(\mathbf{x}, \cdot))_{H(\Phi, \mathbb{R})} && \text{for all } \mathbf{x} \in \Omega \text{ and all } f \in H(\Phi, \mathbb{R}). \end{aligned}$$

The function space $\mathbf{H}(\Omega, \Phi)$ is assumed to be a vector-valued RKHS, i.e. there is an (inner) kernel $\mathbf{K} : \Omega \times \Omega \rightarrow \mathbb{R}^{D \times D}$ such that

$$\begin{aligned} \mathbf{K}(\mathbf{x}, \cdot) \mathbf{c} &\in \mathbf{H}(\Omega, \Phi) && \text{for all } \mathbf{x} \in \Omega \text{ and all } \mathbf{c} \in \mathbb{R}^D, \\ \mathbf{c}^T \mathbf{g}(\mathbf{x}) &= (\mathbf{g}, \mathbf{K}(\mathbf{x}, \cdot) \mathbf{c})_{\mathbf{H}(\Omega, \Phi)} && \text{for all } \mathbf{x} \in \Omega, \text{ all } \mathbf{c} \in \mathbb{R}^D \text{ and all } \mathbf{g} \in \mathbf{H}(\Omega, \Phi). \end{aligned}$$

To formulate the concatenated interpolation problem in the spirit of (1), we have to define an appropriate functional and propose an appropriate search set for the minimization task. To this end, we consider the functional $J : H(\Phi, \mathbb{R}) \times \mathbf{H}(\Omega, \Phi) \rightarrow \mathbb{R}$ given by

$$J(f, \mathbf{g}) := \|f\|_{H(\Phi, \mathbb{R})}^2 + \|\mathbf{g}\|_{\mathbf{H}(\Omega, \Phi)}^2,$$

which penalizes the norms of both the outer and the inner function, and the admissible set

$$\mathcal{A}_{X, Y} := \{(f, \mathbf{g}) \in H(\Phi, \mathbb{R}) \times \mathbf{H}(\Omega, \Phi) \mid f \circ \mathbf{g}(\mathbf{x}_j) = y_j \ 1 \leq j \leq N\} \subset H(\Phi, \mathbb{R}) \times \mathbf{H}(\Omega, \Phi),$$

i.e. the set of all concatenations of functions from $H(\Phi, \mathbb{R})$ and $\mathbf{H}(\Omega, \Phi)$ which interpolate the data. With this notation, we can define the following variational optimization problem

$$J(f, \mathbf{g}) \rightarrow \min \quad \text{for } (f, \mathbf{g}) \in \mathcal{A}_{X,Y} \quad (\text{P})$$

As we explained in section 2, the solution $f_{X,Y}^*$ to the standard interpolation problem (1) can be computed by solving the system (3) of linear equations for a given set of fixed and pairwise disjoint input data points $X := \{\mathbf{x}_1, \dots, \mathbf{x}_N\}$. Therefore, if we assume for a moment that the inner function \mathbf{g} in (P) is fixed and that $Z := \mathbf{g}(X) = \{\mathbf{z}_i = \mathbf{g}(\mathbf{x}_i) \in \Phi \mid i = 1, \dots, N\}$, then we obtain that the solution $f_{Z,Y}^*$ to (1) with data points Z is the only admissible minimizer of the concatenated interpolation problem (P), i.e.

$$f_{Z,Y}^* = \arg \min_{f \in \{h \in H(\Phi, \mathbb{R}) \mid (h, \mathbf{g}) \in \mathcal{A}_{X,Y}\}} \|f\|_{H(\Phi, \mathbb{R})}^2.$$

Note that the coefficients $\boldsymbol{\alpha}^* \in \mathbb{R}^N$ of $f_{Z,Y}^* = \sum_{i=1}^N \alpha_i^* K(\mathbf{z}_i, \cdot)$ can be computed by solving the system

$$\mathbf{M}_{Z,Z} \boldsymbol{\alpha}^* = \mathbf{y}$$

and the value of the optimal energy, i.e. the squared norm, is given by

$$\|f_{Z,Y}^*\|_{H(\Phi, \mathbb{R})}^2 = \boldsymbol{\alpha}^{*T} \mathbf{M}_{Z,Z} \boldsymbol{\alpha}^* = \mathbf{y}^T \mathbf{M}_{Z,Z}^{-1} \mathbf{y}.$$

3.3.1 Application of the representer theorem

In order to rewrite the concatenated interpolation problem (P) into an unconstrained minimization problem by applying the above result, we first have to discuss what happens if $\mathbf{g}(\mathbf{x}_j) = \mathbf{g}(\mathbf{x}_k)$ for two indices $j \neq k$. If equality holds also for the corresponding values from Y , i.e. $y_j = y_k$, we can simply remove the pair $(\mathbf{x}_j, y_j) \in X \times Y$ from the input data and with it also the corresponding condition from the admissible set. However, if $y_j \neq y_k$, there cannot be an $f \in H(\Phi, \mathbb{R})$ such that $(f, \mathbf{g}) \in \mathcal{A}_{X,Y}$. In this case, we simply set $J(f, \mathbf{g}) = \infty$. Using this convention, we can recast (P) into the unrestricted optimization problem

$$J\left(f_{\mathbf{g}(X),Y}^*, \mathbf{g}\right) = \mathbf{y}^T \mathbf{M}_{\mathbf{g}(X),\mathbf{g}(X)}^{-1} \mathbf{y} + \|\mathbf{g}\|_{\mathbf{H}(\Omega, \Phi)}^2 \rightarrow \min \quad \text{for } \mathbf{g} \in \mathbf{H}(\Omega, \Phi) \quad (\text{uP})$$

Therefore, we only have to consider the minimization with respect to $\mathbf{g} \in \mathbf{H}(\Omega, \Phi)$ since the optimal outer function $f_{\mathbf{g}(X),Y}^*$ is completely determined by the inner function values $\mathbf{g}(X)$ and Y .

Note that the side condition $\mathbf{g}(\mathbf{x}_j) \neq \mathbf{g}(\mathbf{x}_k)$ for $j \neq k$ can also be enforced by adding a penalty term of type $\sum_{i < j} W(\|\mathbf{g}(\mathbf{x}_i) - \mathbf{g}(\mathbf{x}_j)\|_2^2)$ to J , where W is a smooth function with $W(0) = \infty$, e.g. $W(x) = \coth(x)$. This can also remedy the problem of small condition numbers of $\mathbf{M}_{\mathbf{g}(X),\mathbf{g}(X)}$ for large sample sizes since it maximizes distances between the point evaluations of \mathbf{g} . Adding this to (uP), we obtain

$$J_\gamma\left(f_{\mathbf{g}(X),Y}^*, \mathbf{g}\right) := J\left(f_{\mathbf{g}(X),Y}^*, \mathbf{g}\right) + \gamma \sum_{1 \leq i < j \leq N} \coth\left(\|\mathbf{g}(\mathbf{x}_i) - \mathbf{g}(\mathbf{x}_j)\|_2^2\right) \rightarrow \min \quad \text{for } \mathbf{g} \in \mathbf{H}(\Omega, \Phi). \quad (12)$$

However, since using $J_0 = J$ in our experiments in section 4 works out well and the side condition does not seem to affect the results for moderate sample sizes, we restrict ourselves to the problem (uP) in the following.

Although the above considerations seem to simplify the concatenated interpolation problem, we still have to solve a highly nonlinear optimization problem over the (possibly) infinite-dimensional RKHS $\mathbf{H}(\Omega, \Phi)$. Nonetheless, by applying Theorem 9 to the unrestricted, concatenated interpolation problem (uP), we can restrict the search space $\mathbf{H}(\Omega, \Phi)$ to the span of the kernel translates in the input data. This has to be understood in the same manner as the standard representer theorem for interpolation, which allows to recast (1) into a finite-dimensional problem with solution (2), see also [19].

Corollary 2. Let $V_X := \text{span}\{\mathbf{K}(\mathbf{x}_i, \cdot)\mathbf{e}_j \mid i = 1, \dots, N \text{ and } j = 1, \dots, D\}$, where \mathbf{e}_j denotes the j -th unit vector in \mathbb{R}^D . Then, the solution \mathbf{g}^* to the unconstrained concatenated interpolation problem (uP) fulfills $\mathbf{g}^* \in V_X$.

Proof. We apply Theorem 1 with $L = 2$, $\Theta_1(x) = \Theta_2(x) = x$ and

$$\mathcal{L}((y_1, f \circ \mathbf{g}(\mathbf{x}_1)), \dots, (y_N, f \circ \mathbf{g}(\mathbf{x}_N))) = \begin{cases} 0 & \text{if } f \circ \mathbf{g}(\mathbf{x}_j) = y_j \ \forall j = 1, \dots, N \\ \infty & \text{else} \end{cases},$$

which exactly resembles the interpolation problem (uP). \square

Due to Corollary 2, we can recast the unrestricted concatenated interpolation problem (uP) into

$$J\left(f_{\mathbf{g}(X), Y}^*, \mathbf{g}\right) = \mathbf{y}^T \mathbf{M}_{\mathbf{g}(X), \mathbf{g}(X)}^{-1} \mathbf{y} + \|\mathbf{g}\|_{\mathbf{H}(\Omega, \Phi)}^2 \rightarrow \min \text{ for } \mathbf{g} \in V_X \subset \mathbf{H}(\Omega, \Phi) \quad (\text{uP-X})$$

This is a nonlinear, finite-dimensional and unrestricted optimization problem. To solve (uP-X), we fix the basis $\{\mathbf{K}(\mathbf{x}_j, \cdot)\mathbf{e}_\ell \mid (j, \ell) \in \mathcal{I}\}$ with $\mathcal{I} := \{(j, \ell) \in \mathbb{N}^2 \mid 1 \leq j \leq N, 1 \leq \ell \leq D\}$. Then, the optimal solution can be written as

$$\mathbf{g}^*(\cdot) = \sum_{(j, \ell) \in \mathcal{I}} c_{j, \ell}^* \mathbf{K}(\mathbf{x}_j, \cdot) \mathbf{e}_\ell. \quad (13)$$

In order to express the minimization problem (uP-X) with respect to the coefficients $\mathbf{c}^* = (c_{1,1}^*, \dots, c_{N,D}^*)^T$, we introduce

$$\mathbf{Q}_{X, X}(\mathbf{c}) := \mathbf{M}_{\mathbf{g}(X), \mathbf{g}(X)} = \left(K \left(\sum_{(j, \ell) \in \mathcal{I}} c_{j, \ell} \mathbf{K}(\mathbf{x}_j, \mathbf{x}_n) \mathbf{e}_\ell, \sum_{(j, \ell) \in \mathcal{I}} c_{j, \ell} \mathbf{K}(\mathbf{x}_j, \mathbf{x}_m) \mathbf{e}_\ell \right) \right)_{1 \leq n, m \leq N} \quad (14)$$

and the corresponding quadratic form

$$\mathcal{Q} : \mathbb{R}^{ND} \rightarrow \mathbb{R}, \quad \mathbf{c} \mapsto \mathbf{y}^T \mathbf{Q}_{X, X}(\mathbf{c})^{-1} \mathbf{y}.$$

Furthermore, to express $\|\mathbf{g}^*\|_{\mathbf{H}(\Omega, \Phi)}^2$ with respect to \mathbf{c}^* , we need

$$\mathcal{N} : \mathbb{R}^{ND} \rightarrow \mathbb{R}, \quad \mathbf{c} \mapsto \sum_{j, k=1}^N \begin{pmatrix} c_{j,1} \\ \vdots \\ c_{j,D} \end{pmatrix}^T \mathbf{K}(\mathbf{x}_j, \mathbf{x}_k) \begin{pmatrix} c_{k,1} \\ \vdots \\ c_{k,D} \end{pmatrix}. \quad (15)$$

Finally, we obtain the optimization problem

$$\mathbf{c}^* = \arg \min_{\mathbf{c} \in \mathbb{R}^{ND}} \underbrace{\mathcal{Q}(\mathbf{c})}_{\|f_{\mathbf{g}(X), Y}^*\|_{\mathbf{H}(\Phi, \mathbb{R})}^2} + \underbrace{\mathcal{N}(\mathbf{c})}_{\|\mathbf{g}\|_{\mathbf{H}(\Omega, \Phi)}^2}. \quad (\text{Int})$$

3.3.2 Solving the minimization problem

The unconstrained problem (Int) is highly nonlinear because the coefficients $c_{j, \ell}$ are transformed by the outer kernel function K . It can be tackled by any suitable iterative optimization algorithm. If the kernels K and \mathbf{K} are differentiable, a quasi-Newton approach is appropriate. If this is not the case, a derivative-free optimizer should be chosen.

Note that we can restrict the minimization in (Int) to a compact subset of \mathbb{R}^{ND} without loss of generality. To this end, let $\underline{\mathbf{K}} \in \mathbb{R}^{ND \times ND}$ be the matrix of matrices $\mathbf{K}(\mathbf{x}_i, \mathbf{x}_j) \in \mathbb{R}^{D \times D}$ and note that

$$\mathcal{Q}(\mathbf{c}) + \mathcal{N}(\mathbf{c}) \geq 0 + \lambda_{\min}(\underline{\mathbf{K}}) \cdot \|\mathbf{c}\|_2^2 \xrightarrow{\|\mathbf{c}\|_2 \rightarrow \infty} \infty,$$

where $\lambda_{\min}(\underline{\mathbf{K}}) > 0$ denotes the smallest eigenvalue of $\underline{\mathbf{K}}$. Therefore, we can restrict our search to the compact set $A := \{\mathbf{c} \in \mathbb{R}^{ND} \mid \|\mathbf{c}\|_2 \leq C\}$ for a large enough $C > 0$. Unfortunately, we cannot directly obtain the existence of a minimizer from this since (Int) is not continuous. However, if we added a smooth term

$$\begin{aligned} \mathcal{P}^\gamma(\mathbf{c}) &= \gamma \sum_{1 \leq m < n \leq N} \coth \left(\|\mathbf{g}(\mathbf{x}_m) - \mathbf{g}(\mathbf{x}_n)\|_2^2 \right) \\ &= \gamma \sum_{1 \leq m < n \leq N} \coth \left(\left\| \sum_{(j,\ell) \in \mathcal{I}} c_{j,\ell} (\mathbf{K}(\mathbf{x}_j, \mathbf{x}_m) - \mathbf{K}(\mathbf{x}_j, \mathbf{x}_n)) \mathbf{e}_\ell \right\|_2^2 \right), \end{aligned}$$

which is equivalent to (12), for $\gamma > 0$, we could deduce the existence of a minimizer with the direct method from the calculus of variations. To this end, note that for a minimizing sequence $(\mathbf{c}_i)_{i=1}^\infty$ of $\mathcal{Q} + \mathcal{N} + \mathcal{P}^\gamma$, there necessarily exist $i_0 \in \mathbb{N}$ and $C_0 > 0$ such that all mutual squared distances $\|\mathbf{g}(\mathbf{x}_m) - \mathbf{g}(\mathbf{x}_n)\|_2^2$ with $1 \leq m < n \leq N$ are larger than C_0 for all \mathbf{c}_i with $i > i_0$. Therefore, we can restrict the minimization to the compact subdomain

$$A \cap \{\mathbf{c} \in \mathbb{R}^{ND} \mid \|\mathbf{g}(\mathbf{x}_m) - \mathbf{g}(\mathbf{x}_n)\|_2^2 \geq C_0 \text{ for } 1 \leq m < n \leq N\},$$

on which $\mathcal{Q} + \mathcal{N} + \mathcal{P}^\gamma$ is continuous, and the existence of a minimizer follows. Nevertheless, as we explained above, the critical condition $\mathcal{P}^\gamma(\mathbf{c}) = \infty$ is practically never met for moderate data set sizes and, therefore, it is safe to assume that there also exists a minimizer for (Int). Note, however, that, depending on the kernels and the data at hand, there can be many minimizers and the solution to (Int) might not be unique. To reduce the chance of getting stuck in a local minimum, we propose to restart the minimization procedure several times with different starting values for \mathbf{c}^* .

Since we will be dealing with differentiable kernel functions in section 4 and since the derivatives of these kernels can be computed explicitly, we propose a BFGS minimization algorithm to solve (Int). To this end, note that the only derivatives we need are essentially the derivative of the inverse of $\mathbf{Q}_{X,X}(\mathbf{c})$, i.e.

$$\frac{\partial}{\partial c_{m,n}} \mathbf{Q}_{X,X}^{-1}(\mathbf{c}) = -\mathbf{Q}_{X,X}^{-1}(\mathbf{c}) \frac{\partial}{\partial c_{m,n}} \mathbf{Q}_{X,X}(\mathbf{c}) \mathbf{Q}_{X,X}^{-1}(\mathbf{c}),$$

and the derivative of $\mathbf{Q}_{X,X}(\mathbf{c})$, which consists of the derivative of the outer kernel K , which is known analytically for all kernel choices which we discuss in section 4, and

$$\frac{\partial}{\partial c_{m,n}} \mathbf{g}(\mathbf{x}) = \frac{\partial}{\partial c_{m,n}} \sum_{(j,\ell) \in \mathcal{I}} c_{j,\ell} \mathbf{K}(\mathbf{x}_j, \mathbf{x}) \mathbf{e}_\ell = \mathbf{K}(\mathbf{x}_m, \mathbf{x}) \mathbf{e}_n$$

for each $(m,n) \in \mathcal{I}$. The overall computational cost complexity for one BFGS step, i.e. evaluation of \mathcal{Q}, \mathcal{N} and their derivatives, is bounded by $\mathcal{O}(N^3D + (ND)^2)$.

3.4 Least-squares regression

For concatenated, regularized least-squares regression, the minimization task changes to

$$J_{\lambda,\mu}(f, \mathbf{g}) := \sum_{j=1}^N |f \circ \mathbf{g}(\mathbf{x}_j) - y_j|^2 + \lambda \|f\|_{H(\Phi, \mathbb{R})}^2 + \mu \|\mathbf{g}\|_{\mathbf{H}(\Omega, \Phi)}^2 \rightarrow \min \text{ for } f \in H(\Phi, \mathbb{R}), \mathbf{g} \in \mathbf{H}(\Omega, \Phi) \quad (\text{R})$$

with $\lambda, \mu > 0$, which is in the same fashion as the standard least-squares regression problem (5).

Analogously to our considerations in section 3.3, we find that, for fixed inner points $Z = \mathbf{g}(X) \subset \Phi$, the function $f_{Z,Y}^\lambda$, see (5), is the solution of the problem

$$\sum_{j=1}^N |f(z_j) - y_j|^2 + \lambda \|f\|_{H(\Phi, \mathbb{R})}^2 \rightarrow \min \text{ for } f \in H(\Phi, \mathbb{R}).$$

The corresponding coefficients $\boldsymbol{\alpha}^\lambda \in \mathbb{R}^N$ with respect to the basis $\{K(z_j, \cdot) \mid j = 1, \dots, N\}$ are computed by solving

$$(\mathbf{M}_{Z,Z} + \lambda \mathbf{I}) \boldsymbol{\alpha}^\lambda = \mathbf{y}.$$

Therefore, each of the terms of the optimal energy can be expressed as

$$\begin{aligned} \|f_{Z,Y}^\lambda\|_{H(\Phi, \mathbb{R})}^2 &= \boldsymbol{\alpha}^{\lambda T} \mathbf{M}_{Z,Z} \boldsymbol{\alpha}^\lambda = \mathbf{y}^T (\mathbf{M}_{Z,Z} + \lambda \mathbf{I})^{-1} \mathbf{M}_{Z,Z} (\mathbf{M}_{Z,Z} + \lambda \mathbf{I})^{-1} \mathbf{y}, \\ \sum_{j=1}^N |f_{Z,Y}^\lambda(z_j) - y_j|^2 &= \|\mathbf{M}_{Z,Z} \boldsymbol{\alpha}^\lambda - \mathbf{y}\|_2^2 = \left\| \left(\mathbf{I} - \mathbf{M}_{Z,Z} (\mathbf{M}_{Z,Z} + \lambda \mathbf{I})^{-1} \right) \mathbf{y} \right\|_2^2. \end{aligned}$$

3.4.1 Application of the representer theorem

Analogously to (uP), we can use

$$\begin{aligned} J_{\lambda, \mu} \left(f_{\mathbf{g}(X), Y}^\lambda, \mathbf{g} \right) &= \lambda \mathbf{y}^T (\mathbf{M}_{\mathbf{g}(X), \mathbf{g}(X)} + \lambda \mathbf{I})^{-1} \mathbf{M}_{\mathbf{g}(X), \mathbf{g}(X)} (\mathbf{M}_{\mathbf{g}(X), \mathbf{g}(X)} + \lambda \mathbf{I})^{-1} \mathbf{y} + \mu \|\mathbf{g}\|_{\mathbf{H}(\Omega, \Phi)}^2 \\ &\quad + \left\| \left(\mathbf{I} - \mathbf{M}_{\mathbf{g}(X), \mathbf{g}(X)} (\mathbf{M}_{\mathbf{g}(X), \mathbf{g}(X)} + \lambda \mathbf{I})^{-1} \right) \mathbf{y} \right\|_2^2 \end{aligned} \quad (16)$$

to reformulate (R) as

$$J_{\lambda, \mu} \left(f_{\mathbf{g}(X), Y}^\lambda, \mathbf{g} \right) \rightarrow \min \text{ for } \mathbf{g} \in \mathbf{H}(\Omega, \Phi). \quad (\text{uR})$$

Corollary 3. *The solution $\mathbf{g}^{\lambda, \mu}$ to the unconstrained concatenated regression problem (uR) fulfills $\mathbf{g}^{\lambda, \mu} \in V_X$.*

Proof. We apply Theorem 1 with $L = 2$, $\Theta_1(x) = \lambda \cdot x$, $\Theta_2(x) = \mu \cdot x$ and

$$\mathcal{L}((y_1, f \circ \mathbf{g}(\mathbf{x}_1)), \dots, (y_N, f \circ \mathbf{g}(\mathbf{x}_N))) = \sum_{j=1}^N |f \circ \mathbf{g}(\mathbf{x}_j) - y_j|^2,$$

which resembles the regression problem (R). □

Hence, as for interpolation, we obtain a representer theorem for concatenated least-squares regression, which allows us to replace the infinite-dimensional optimization problem (R) with the finite-dimensional problem

$$J_{\lambda, \mu} \left(f_{\mathbf{g}(X), Y}^\lambda, \mathbf{g} \right) \rightarrow \min \text{ for } \mathbf{g} \in V_X \subset \mathbf{H}(\Omega, \Phi). \quad (\text{uR-X})$$

Finally, we want to express (uR-X) in terms of the coefficients $\mathbf{c}^{\lambda, \mu} = (c_{1,1}^{\lambda, \mu}, \dots, c_{N,D}^{\lambda, \mu})^T$ of $\mathbf{g}^{\lambda, \mu}$ with respect to the basis $\{\mathbf{K}(\mathbf{x}_j, \cdot) \mathbf{e}_\ell \mid (j, \ell) \in \mathcal{I}\}$. To this end, we define the quadratic forms

$$\begin{aligned} \mathcal{Q}^\lambda : \mathbb{R}^{ND} &\rightarrow \mathbb{R}, \quad \mathbf{c} \mapsto \lambda \cdot \mathbf{y}^T (\mathbf{Q}_{X,X}(\mathbf{c}) + \lambda \mathbf{I})^{-1} \mathbf{Q}_{X,X}(\mathbf{c}) (\mathbf{Q}_{X,X}(\mathbf{c}) + \lambda \mathbf{I})^{-1} \mathbf{y}, \\ \mathcal{N}^\mu : \mathbb{R}^{ND} &\rightarrow \mathbb{R}, \quad \mathbf{c} \mapsto \mu \cdot \mathcal{N}(\mathbf{c}) \quad \text{and} \\ \mathcal{C}^\lambda : \mathbb{R}^{ND} &\rightarrow \mathbb{R}, \quad \mathbf{c} \mapsto \mathbf{y}^T \left(\mathbf{I} - \mathbf{Q}_{X,X}(\mathbf{c}) (\mathbf{Q}_{X,X}(\mathbf{c}) + \lambda \mathbf{I})^{-1} \right)^T \left(\mathbf{I} - \mathbf{Q}_{X,X}(\mathbf{c}) (\mathbf{Q}_{X,X}(\mathbf{c}) + \lambda \mathbf{I})^{-1} \right) \mathbf{y} \end{aligned}$$

with the help of (14) and (15). Subsequently, we arrive at the optimization problem

$$\mathbf{c}^{\lambda,\mu} = \arg \min_{\mathbf{c} \in \mathbb{R}^{ND}} \mathcal{Q}^\lambda(\mathbf{c}) + \mathcal{N}^\mu(\mathbf{c}) + \mathcal{C}^\lambda(\mathbf{c}), \quad (\text{Reg})$$

which is the equivalent to (uR-X).

3.4.2 Solving the minimization problem

Note that the existence of a minimizer follows by similar arguments as in the previous section for the interpolation problem, i.e.

$$\mathcal{Q}^\lambda(\mathbf{c}) + \mathcal{N}^\mu(\mathbf{c}) + \mathcal{C}^\lambda(\mathbf{c}) \geq \mu \cdot \lambda_{\min}(\mathbf{K}) \cdot \|\mathbf{c}\|_2^2 \xrightarrow{\|\mathbf{c}\|_2 \rightarrow \infty} \infty$$

and, thus, we can restrict the search for a minimizer to a compact subset of \mathbb{R}^{ND} . For regression, we need the inverse of $\mathbf{Q}_{X,X}(\mathbf{c}) + \lambda\mathbf{I}$ to compute \mathcal{Q}^λ , which is positive definite for every $\lambda > 0$ and, therefore, there are no pathological cases as in the interpolation setting. Thus, the functions $\mathcal{Q}^\lambda, \mathcal{N}^\mu, \mathcal{C}^\lambda$ are continuous and the minimization of (Reg) over a compact subset of \mathbb{R}^{ND} has a minimizer. Nevertheless, also in this case the minimizer is not necessarily unique.

If the kernel functions are differentiable, we can again employ a BFGS algorithm with several restarts to find the optimal coefficients $\mathbf{c}^{\lambda,\mu}$. To this end, note that \mathcal{Q}^λ and \mathcal{N}^μ can be computed similarly as \mathcal{Q} and \mathcal{N} in the interpolation case. Furthermore, also the derivative of \mathcal{C}^λ can be computed with the same techniques since we essentially only need the derivatives of $\mathbf{Q}_{X,X}(\mathbf{c})$ and $(\mathbf{Q}_{X,X}(\mathbf{c}) + \lambda\mathbf{I})^{-1}$. While the number of terms is larger than in the interpolation case, the asymptotic computational runtime is still bounded by $\mathcal{O}(N^3D + (ND)^2)$. Furthermore, the condition number of the matrix $\mathbf{Q}_{X,X}(\mathbf{c}) + \lambda\mathbf{I}$ is smaller than the one of $\mathbf{Q}_{X,X}$, which had to be inverted for interpolation. Therefore, computing $\mathcal{Q}^\lambda(\mathbf{c})$ with an iterative solver for the application of $(\mathbf{Q}_{X,X}(\mathbf{c}) + \lambda\mathbf{I})^{-1}$ needs fewer computational steps than computing $\mathcal{Q}(\mathbf{c})$ in the interpolation case.

Finally, let us remark that for both interpolation and least-squares regression there exists another possibility to obtain a finite-dimensional optimization problem from (P) and (R), respectively, without using the representer theorem. We could discretize the functions $f_1 \in \mathcal{H}_1$ and $f_2 \in \mathcal{H}_2$ by $\tilde{f}_1 \in V_1$ and $\tilde{f}_2 \in V_2$ with finite-dimensional spaces V_1, V_2 , see e.g. [3] for an error analysis of this scenario for single-layer regression. However, when following this approach, the choice of the discretization can severely influence the results of the minimization. Furthermore, we are restricted in the size of the dimensions of the discretization spaces V_1, V_2 , which influences the computational costs for solving the underlying optimization problem.

4 Experiments

This section serves to provide numerical examples on the performance of the two-layer interpolation and regression algorithms presented in the previous section. Note that the image Φ of the inner function space has to be compatible with the domain of the outer function space. For reasons of simplicity, we will stick to outer function spaces $H(\Phi, \mathbb{R})$ which are defined on the whole space \mathbb{R}^D . Furthermore, we assume that the matrix-valued kernel $\mathbf{K} : \Omega \times \Omega \rightarrow \mathbb{R}^{D \times D}$ of the inner RKHS can be written as

$$\mathbf{K}(\mathbf{x}, \mathbf{y}) = K_{\mathcal{I}}(\mathbf{x}, \mathbf{y}) \cdot \text{diag}(\mathbf{a})$$

for some weight vector $\mathbf{a} \in \mathbb{R}_+^D$. Here, $\text{diag}(\mathbf{a})$ denotes the diagonal matrix \mathbf{A} with $A_{ii} = \mathbf{a}_i$ and $K_{\mathcal{I}} : \Omega \times \Omega \rightarrow \mathbb{R}$ is a scalar-valued kernel function.

Possible outer and inner kernel functions K and $K_{\mathcal{I}}$ are the polynomial kernel

$$K_{\text{Poly},p}(\mathbf{x}, \mathbf{y}) := (\mathbf{x}^T \mathbf{y} + 1)^p,$$

the Gaussian kernel

$$K_{\text{Gauss},\sigma}(\mathbf{x}, \mathbf{y}) := \exp\left(-\frac{\|\mathbf{x} - \mathbf{y}\|^2}{2\sigma^2}\right)$$

and the Matérn kernel

$$K_{\text{Matérn},s}(\mathbf{x}, \mathbf{y}) := \kappa_{\frac{2s-1}{2}}(\|\mathbf{x} - \mathbf{y}\|) \cdot \|\mathbf{x} - \mathbf{y}\|^{\frac{2s-1}{2}},$$

where κ_α denotes the modified (hyperbolic) Bessel function of second kind with parameter α . Note that the latter characterizes the Sobolev space of order $s \in \mathbb{N}$, see e.g. [9]. Furthermore, for illustrative reasons, we also have a look at the corresponding tensor-product kernel

$$K_{\text{TensorMatérn},\hat{s}}(\mathbf{x}, \mathbf{y}) := \prod_{i=1}^d \kappa_{\frac{2\hat{s}-1}{2}}(|x_i - y_i|) \cdot |x_i - y_i|^{\frac{2\hat{s}-1}{2}}.$$

This tensor-product Matérn kernel is directly related to the Sobolev spaces of dominating mixed smoothness, which play an important role for hyperbolic cross or sparse grid approximations for instance, see e.g. [4]. Note that the Gaussian kernel is already a tensor product kernel by nature. Choosing a tensor-product kernel of polynomials instead of K_{Poly} did not significantly change the results we achieved. Therefore, we omit it here.

4.1 Reconstruction error

Let us choose $\Omega = [-1, 1]^2$. We will evaluate our method for the two test functions

$$\begin{aligned} h_1 : \Omega &\rightarrow \mathbb{R} & h_1(x, y) &:= (0.1 + |x - y|)^{-1} \\ h_2 : \Omega &\rightarrow \mathbb{R} & h_2(x, y) &:= \begin{cases} 1 & \text{if } x \cdot y > \frac{3}{20} \\ 0 & \text{else} \end{cases}. \end{aligned}$$

The function h_1 employs a kink-like structure along the diagonal of the domain, while h_2 represents an indicator function with a jump. Neither of these two functions is an element of a reproducing kernel space spanned by any of the above kernel functions³ for arbitrary parameters $p, s \in \mathbb{N}, \sigma \in (0, \infty)$. Therefore they cannot be approximated too well by a single-layer method. The approximation of such functions with kinks or jumps by (a composition of) smooth functions plays an important role in applications from econometrics or two-phase flow problems for example. To handle the latter with a level-set approach the discontinuous material parameters have to be smoothed out by a level-set function, see e.g. chapter 4 of [6].

We first choose $D = d = 2$, i.e. $\Omega, \Phi \subset \mathbb{R}^2$, and $\mathbf{a} = (1 \ 1)^T$. We then draw $N = 100$ random equidistributed points $\{\mathbf{x}_1, \dots, \mathbf{x}_N\} \subset \Omega$ independently and set $y_i := h_*(\mathbf{x}_i) + \varepsilon_i$ for all $i = 1, \dots, N$ for the benchmark function $h_* \in \{h_1, h_2\}$. Here, ε_i are additive noise perturbations which are drawn i.i.d. according to a centered Gaussian distribution with standard deviation 0.01. To solve (Int) or (Reg), respectively, we use a BFGS algorithm with random initialization of the coefficient vector \mathbf{c} of the inner function, see also (13). As the goal functions employ many local minima, we always run the algorithm 64 times and pick the vector \mathbf{c} (and with this the functions f and \mathbf{g}) for which the smallest goal function value in (Int) or (Reg), respectively, is achieved.

To be able to compare our computed $f(g(\cdot))$, which approximates the true solution $f_{\mathbf{g}(X),Y}^*(\mathbf{g}^*(\cdot))$ or $f_{\mathbf{g}(X),Y}^\lambda(\mathbf{g}^{\lambda,\mu}(\cdot))$, respectively, to the result of a standard kernel interpolation/regression, we also calculate the interpolant/regressor w in the reproducing kernel Hilbert space $H(\Omega, \mathbb{R})$ which employs the same kernel type and parameters as $H(\Phi, \mathbb{R})$, but on a different domain Ω instead of Φ . We then measure an

³Note that h_1 is an element of the Sobolev space $H^1(\Omega)$ of order 1. However, this space is not an RKHS for $d = 2$ due to the Sobolev embedding theorem.

approximation to the L_2 reconstruction error by

$$E_{f,g} := \sqrt{\frac{1}{n_t} \sum_{i=1}^{n_t} (f \circ \mathbf{g} - h_*)^2(\mathbf{t}_i)} \quad \text{and} \quad E_w := \sqrt{\frac{1}{n_t} \sum_{i=1}^{n_t} (w - h_*)^2(\mathbf{t}_i)}.$$

Here, \mathbf{t}_i are the points of a uniform grid of meshwidth $\frac{1}{50}$ over $\Omega = [-1, 1]^2$, i.e. $n_t = 101^2$. We also consider the *pointwise error*

$$|(f \circ \mathbf{g} - h_*)(\mathbf{t}_i)| \quad \text{and} \quad |(w - h_*)(\mathbf{t}_i)|$$

for $i = 1, \dots, n_t$ in a two-dimensional contour plot.

4.1.1 Interpolation

We first compare the results for two-layer interpolation, see (Int), with the results for single-layer interpolation, see (1). In Figures 3, 4, 5 and 6 we displayed the pointwise errors for several combinations of outer and inner functions. The corresponding L_2 reconstruction errors $E_{f,g}$ and E_w can be found in Table 1. Note that we choose smoothness $s = 2$ for the Matérn spaces since this is the smallest $s \in \mathbb{N}$ for which the corresponding space is an RKHS with $d = 2$. However, in the tensor-product case, we choose $\hat{s} = 1$, which also results in an RKHS, regardless of the dimension d .

In Figures 3 and 4, we can observe the errors for interpolation with an outer Matérn kernel or tensor-product Matérn kernel, respectively, and inner polynomial kernels of degrees 1 and 2. We directly observe that there is a significant improvement in the error when dealing with two-layer interpolation instead of single-layer interpolation. While the benefits of two-layer interpolation are already observable for the test function h_2 , they become even more obvious for h_1 . As we explained in the beginning of section 3, the fact that the kink of h_1 is not parallel to a coordinate axis poses a problem when dealing with the tensor-product kernel. Since a linear transformation (rotation) would suffice to remedy this problem, the polynomial kernel of degree $p = 1$ already suffices to obtain a better error behavior. Therefore, $p = 2$ can already lead to a small overfitting effect as we observe in Figure 4. Nevertheless, the error is still significantly better than in the single-layer case. In the case of h_2 , however, we have a jump alongside nonlinear curves. Here, $p = 2$ seems to be more appropriate to deal with this problem.

In the case of an outer Matérn kernel and an inner Gaussian kernel we see similar improvements for the two-layer case in Figure 5. Note however, that the Gaussian kernel width is quite crucial to obtain good results. As we see, $\sigma = 10$ does not lead to significantly better results than in the single-layer case, whereas $\sigma = 1$ does.

Finally, we choose an outer Gaussian kernel with $\sigma = 0.1$ and again use polynomial kernels of degrees $p = 1$ and $p = 2$ for the inner function. Here, we deliberately set the kernel width of the outer kernel to a small value such that the single-layer interpolation does not achieve good results. As we observe in Figure 6, the two-layer-scheme is able to remedy also the bad parameter choice of the outer kernel. Here, especially the improvements for the test function h_2 are remarkable.

Overall, we come to the conclusion that interpolation in reproducing kernel Hilbert spaces significantly benefits from a two-layer approach if the reproducing kernel at hand does not suit the underlying function.

4.1.2 Regression

Now we have a look at the errors for solving the least-squares regression problem (Reg) with the same kernel choices as above. To determine the optimal parameters λ and μ , we run a 5-fold cross-validation on the input data for all possible choices $\lambda, \mu \in \{2^{-2t+1} \mid t = 1, \dots, 10\}$. Subsequently, we use the parameter pair (λ, μ) for which the smallest function value of (Reg) is achieved and run the regression algorithm on the whole input data set to obtain our final results. We compare the two-layer case with the single-layer regression,

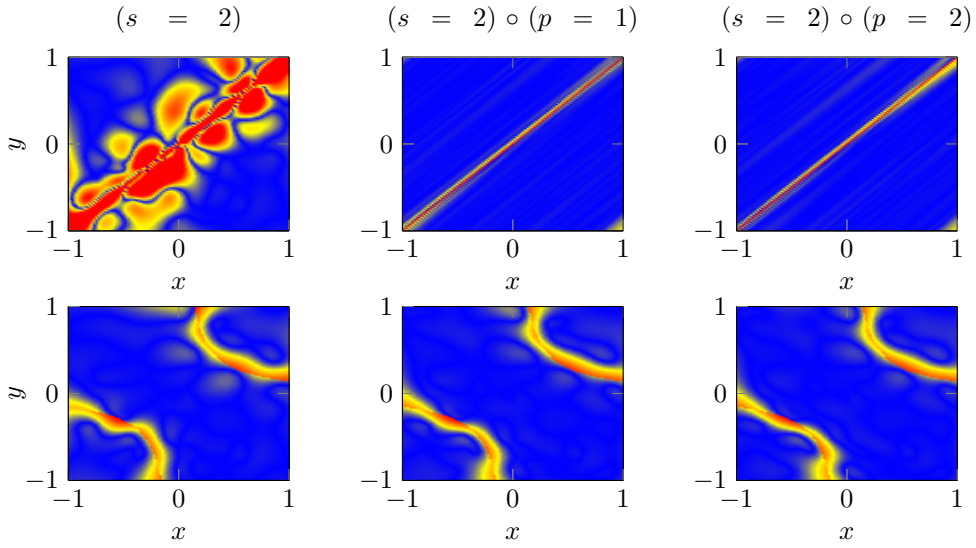


Figure 3: The pointwise error for standard interpolation (left) and for concatenated interpolation with outer kernel $K_{\text{Matérn},1}$ and inner kernel $K_{\text{Poly},1}$ (mid) or $K_{\text{Poly},2}$ (right), respectively. We plotted both, the error for h_1 (top) and h_2 (bottom). The color scale ranges from blue (0% error) to red (more than 10% error), where the percentage has to be understood with respect to the $\|\cdot\|_{L_\infty}$ norm of h_1 or h_2 , respectively.

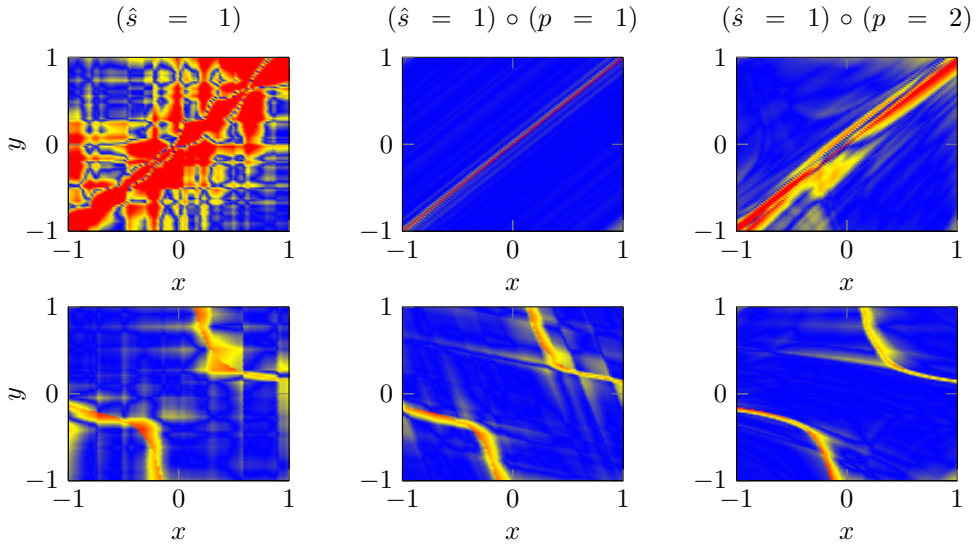


Figure 4: The pointwise error for standard interpolation (left) and for concatenated interpolation with outer kernel $K_{\text{TensorMatérn},1}$ and inner kernel $K_{\text{Poly},1}$ (mid) or $K_{\text{Poly},2}$ (right), respectively. We plotted both, the error for h_1 (top) and h_2 (bottom). The color scale ranges from blue (0% error) to red (more than 10% error), where the percentage has to be understood with respect to the $\|\cdot\|_{L_\infty}$ norm of h_1 or h_2 , respectively.

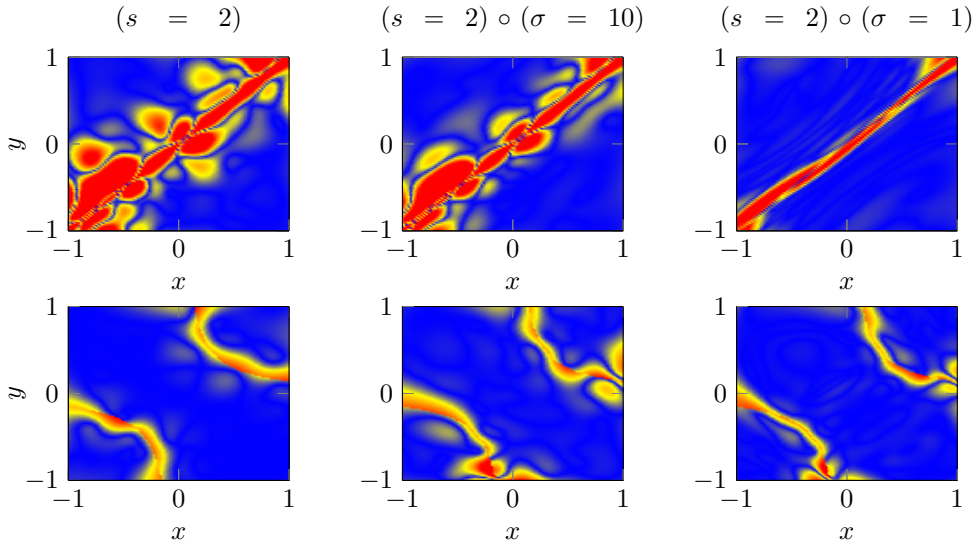


Figure 5: The pointwise error for standard interpolation (left) and for concatenated interpolation with outer kernel $K_{\text{Matérn},2}$ and inner kernel $K_{\text{Gauss},10}$ (mid) or $K_{\text{Gauss},1}$ (right), respectively. We plotted both, the error for h_1 (top) and h_2 (bottom). The color scale ranges from blue (0% error) to red (more than 10% error), where the percentage has to be understood with respect to the $\|\cdot\|_{L_\infty}$ norm of h_1 or h_2 , respectively.

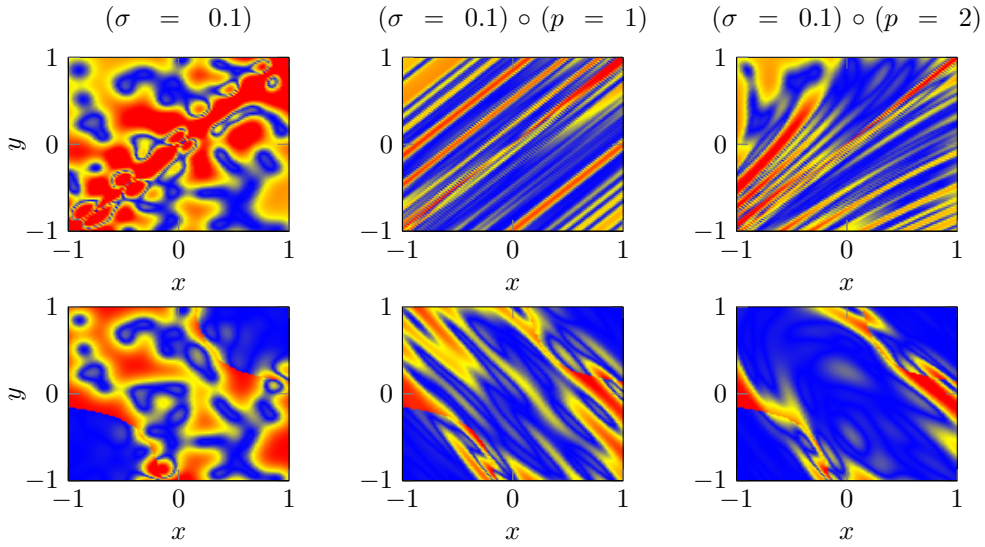


Figure 6: The pointwise error for standard interpolation (left) and for concatenated interpolation with outer kernel $K_{\text{Gauss},0.1}$ and inner kernel $K_{\text{Poly},1}$ (mid) or $K_{\text{Poly},2}$ (right), respectively. We plotted both, the error for h_1 (top) and h_2 (bottom). The color scale ranges from blue (0% error) to red (more than 10% error), where the percentage has to be understood with respect to the $\|\cdot\|_{L_\infty}$ norm of h_1 or h_2 , respectively.

	Mat \circ Poly			Mat-TP \circ Poly		
Errors	E_h	$E_{f,g}(p=1)$	$E_{f,g}(p=2)$	E_h	$E_{f,g}(\sigma=1)$	$E_{f,g}(\sigma=0.1)$
h_1	0.9184	0.1283	0.1282	1.2548	0.1462	0.3693
h_2	0.1571	0.1517	0.1500	0.1683	0.1316	0.1100

	Mat \circ Gauss			Gauss \circ Poly		
Errors	E_h	$E_{f,g}(\sigma=10)$	$E_{f,g}(\sigma=1)$	E_h	$E_{f,g}(p=1)$	$E_{f,g}(p=2)$
h_1	0.9562	0.8013	0.4153	1.0894	0.3662	0.3882
h_2	0.2142	0.2003	0.1534	0.4179	0.2980	0.2495

Table 1: Errors for interpolation.

see also (5), with the parameter λ , which achieves the smallest error, i.e. we compare to the best possible single-layer solution.

As we observe in Figures 7, 8, 9, 10 and Table 2, the qualitative results are very similar to the interpolation case. Again, we observe a significant improvement of the two-layer approach over the single-layer one. Here, it is remarkable that the two-layer results, which have been achieved by crossvalidation on the training data, are always equally good or even better than the single-layer results with the optimal regularization parameter determined on the test set. Therefore, we can say that the two-layer approach performs better than the best possible single-layer approach for regularized least-squares regression.

	Mat \circ Poly			Mat-TP \circ Poly		
Errors	E_h	$E_{f,g}(p=1)$	$E_{f,g}(p=2)$	E_h	$E_{f,g}(\sigma=1)$	$E_{f,g}(\sigma=0.1)$
h_1	0.9184	0.1436	0.1288	1.2352	0.1379	0.3553
h_2	0.1564	0.1579	0.1422	0.1743	0.1752	0.1727

	Mat \circ Gauss			Gauss \circ Poly		
Errors	E_h	$E_{f,g}(\sigma=10)$	$E_{f,g}(\sigma=1)$	E_h	$E_{f,g}(p=1)$	$E_{f,g}(p=2)$
h_1	0.9184	0.1930	0.4041	1.3998	0.2021	0.1659
h_2	0.1564	0.1570	0.1462	0.3133	0.1593	0.1582

Table 2: Errors for regression.

4.2 Transformation by the inner function

To get a better intuition on how the two-layer algorithms work, we inspect the inner function \mathbf{g} in the case of least-squares regression with an outer tensor-product Matérn kernel and an inner polynomial kernel. To this end, we depict isotropic grid points in $\Omega = [-1, 1]^2$ and have a look how these points are transformed by \mathbf{g} in Figure 11.

As we observe, for h_1 and $p=1$, the inner function reduces the two-dimensional grid to a one-dimensional line. The kink of the original function h_1 now resides in the mid point of this line. Therefore, one can easily characterize the kink by the x -coordinate after the inner transformation. This reduces the original two-dimensional kink description $x-y=0$ to just $x=c$ for a fixed $c \in \mathbb{R}$. While the function with the kink along the diagonal does not reside in the tensor-product Matérn space of order 1, which corresponds to the outer kernel in this example, a function with a kink parallel to one of the coordinate axes does. Therefore, the inner function \mathbf{g} transforms the domain in such a way that the result resides in the RKHS to which the outer function belongs. While there is no reduction to a one-dimensional line in the case $p=2$, the principle remains the same. The inner function aligns the kink almost perpendicular to the x -axis. However, having

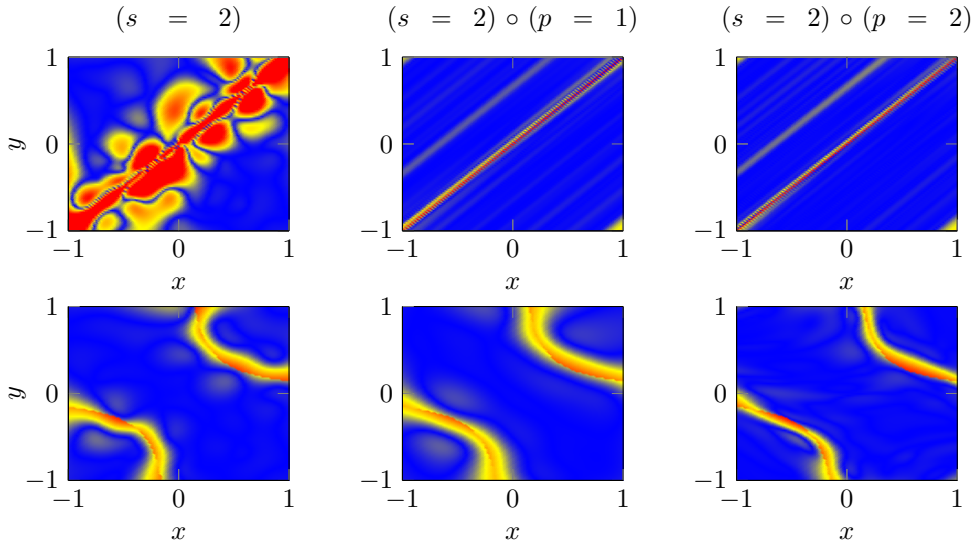


Figure 7: The pointwise error for standard least-squares (left) and for concatenated least-squares with outer kernel $K_{\text{Matérn},1}$ and inner kernel $K_{\text{Poly},1}$ (mid) or $K_{\text{Poly},2}$ (right), respectively. We plotted both, the error for h_1 (top) and h_2 (bottom). The color scale ranges from blue (0% error) to red (more than 10% error), where the percentage has to be understood with respect to the $\|\cdot\|_{L_\infty}$ norm of h_1 or h_2 , respectively.

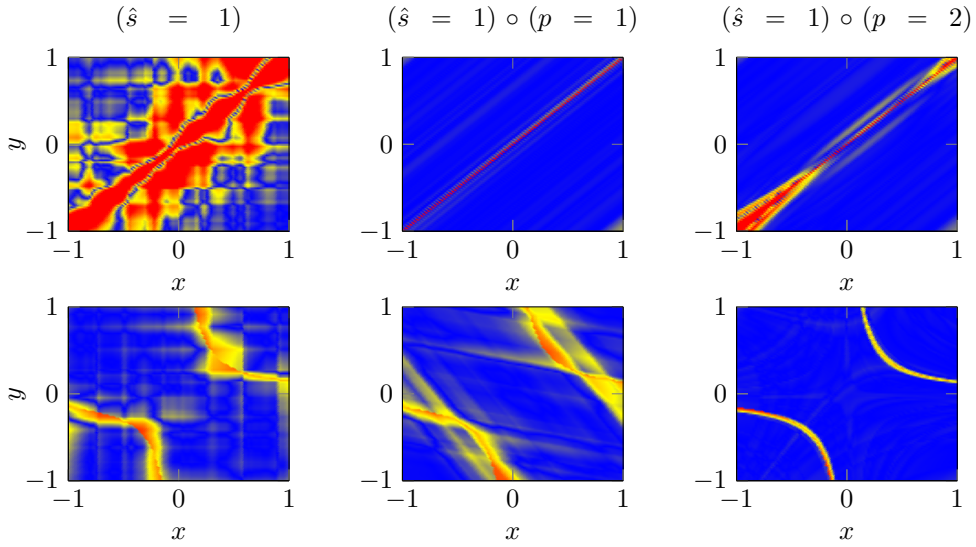


Figure 8: The pointwise error for standard least-squares (left) and for concatenated least-squares with outer kernel $K_{\text{TensorMatérn},1}$ and inner kernel $K_{\text{Poly},1}$ (mid) or $K_{\text{Poly},2}$ (right), respectively. We plotted both, the error for h_1 (top) and h_2 (bottom). The color scale ranges from blue (0% error) to red (more than 10% error), where the percentage has to be understood with respect to the $\|\cdot\|_{L_\infty}$ norm of h_1 or h_2 , respectively.

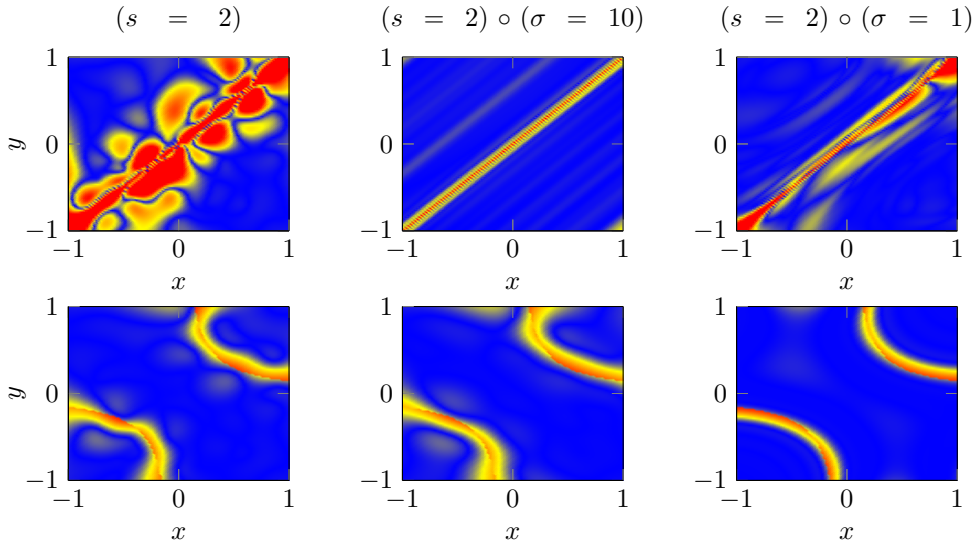


Figure 9: The pointwise error for standard least-squares (left) and for concatenated least-squares with outer kernel $K_{\text{Matérn},2}$ and inner kernel $K_{\text{Gauss},10}$ (mid) or $K_{\text{Gauss},1}$ (right), respectively. We plotted both, the error for h_1 (top) and h_2 (bottom). The color scale ranges from blue (0% error) to red (more than 10% error), where the percentage has to be understood with respect to the $\|\cdot\|_{L_\infty}$ norm of h_1 or h_2 , respectively.

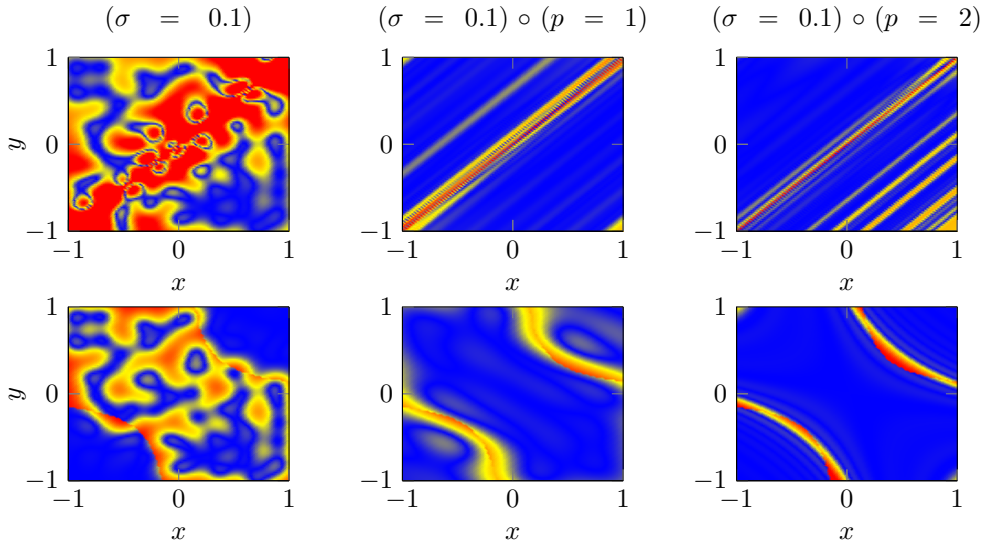


Figure 10: The pointwise error for standard least-squares (left) and for concatenated least-squares with outer kernel $K_{\text{Gauss},0.1}$ and inner kernel $K_{\text{Poly},1}$ (mid) or $K_{\text{Poly},2}$ (right), respectively. We plotted both, the error for h_1 (top) and h_2 (bottom). The color scale ranges from blue (0% error) to red (more than 10% error), where the percentage has to be understood with respect to the $\|\cdot\|_{L_\infty}$ norm of h_1 or h_2 , respectively.

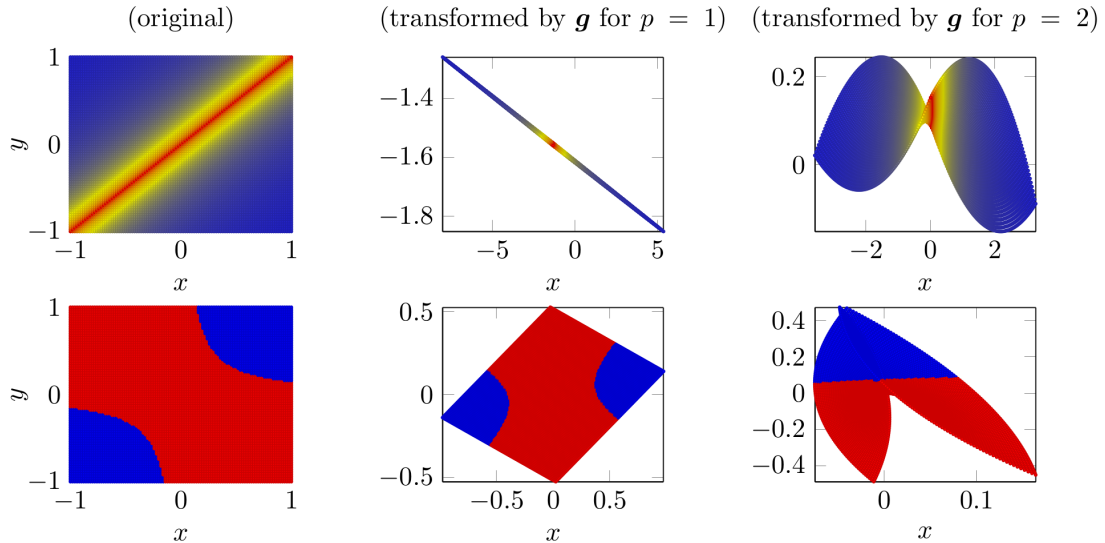


Figure 11: The transformation of the isotropic grid points (left) by the inner function with $p = 1$ (mid) and $p = 2$ (right). The underlying problem is least-squares regression of h_1 (top) and h_2 (bottom) for the outer kernel $K_{\text{TensorMatérn},1}$ and the inner kernel $K_{\text{Poly},p}$. The color scale represents the values of h_1 or h_2 , respectively.

a closer look, one can observe that it is not as perfectly aligned as in the case $p = 1$. Therefore, the error in Figure 8 is slightly larger for $p = 2$.

Considering the test function h_2 , we see that a linear inner transformation, i.e. $p = 1$, essentially just rotates the domain and it does not change the alignment of the jump very much. However, in the case $p = 2$, the inner function \mathbf{g} manages to transform the domain in such a way that the jump is now almost parallel to the x -axis. While we do not observe a significant improvement when considering the overall error in table 2 in this case, the pointwise errors in Figure 8 seem to really benefit from this transformation and the jump is resolved almost perfectly. Overall, we observe that the inner function \mathbf{g} tries to align the features of the original test function in such a way that they can be easily resolved by the outer function f .

5 Conclusion

In this paper, we presented a general representer theorem for concatenated machine learning problems. The statement essentially boils down to the fact that the a priori infinite-dimensional optimization problem, which appears when dealing with function compositions from reproducing kernel Hilbert spaces, can be recast into a finite-dimensional optimization problem, where we only have to deal with at most N kernel translates in each layer of the composition. Here, N denotes the number of input data points. We introduced a simple neural network architecture, which represents the concatenated functions we are dealing with. Furthermore, we established a connection between our representer theorem and two types of state-of-the-art deep learning algorithms, namely multi-layer multiple kernel learning and deep kernel networks. Finally, we presented a detailed analysis on a two-layer interpolation and a two-layer least-squares regression algorithm, which can directly be derived from our representer theorem. We evaluated the results of these algorithms for several settings to illustrate that a multi-layer kernel method is able to remedy the shortcomings of a single-layer variant.

Since the two algorithms presented here are straightforward consequences of the representer theorem for

concatenated functions and only serve to illustrate its application, they are not very sophisticated in terms of runtime efficiency, input data handling and numerical optimization performance. It would be interesting to see if these simple algorithms could be tweaked in such a way that high-dimensional big data problems become accessible and that they might join the ranks of modern deep learning methods, see e.g. [11, 17, 20]. In this context, one could for example think of clever reduction strategies to minimize the number of kernel evaluations as for SVMs, see e.g. [19].

While we were able to explain the success of certain MLMKL algorithms and DKN schemes with our representer theorem, it would be interesting to see if other classes of deep neural networks or even general machine learning algorithms can be interpreted in such a way that Theorem 1 can be applied to them.

Finally, note that it is crucial to our approach that the reproducing kernel spaces at hand stay fixed. In this context, it would be interesting to see if our theorem could be enhanced in such a way that it also includes the optimization of certain hyperparameters of the kernel, e.g. the degree of a polynomial kernel or the width of a Gaussian kernel.

References

- [1] N. Aronszajn, *Theory of reproducing kernels*, Transactions of the American Mathematical Society **68** (1950), no. 3, 337–404.
- [2] F. Bach, G. Lanckriet, and M. Jordan, *Multiple kernel learning, conic duality, and the SMO algorithm*, Proceedings of the 21st International Conference on Machine Learning, 2004, pp. 1–9.
- [3] B. Bohn and M. Griebel, *Error estimates for multivariate regression on discretized function spaces*, SIAM Journal on Numerical Analysis **55** (2017), no. 4, 1843–1866.
- [4] H.-J. Bungartz and M. Griebel, *Sparse grids*, Acta Numerica **13** (2004), 147–269.
- [5] Y. Cho and L. Saul, *Kernel methods for deep learning*, Advances in Neural Information Processing Systems (Y. Bengio, D. Schuurmans, J. Lafferty, C. Williams, and A. Culotta, eds.), vol. 22, Curran Associates, Inc., 2009, pp. 342–350.
- [6] R. Croce, *Numerische Simulation der Interaktion von inkompressiblen Zweiphasenströmungen mit Starrkörpern in drei Raumdimensionen*, Ph.D. thesis, Institut für Numerische Simulation, Universität Bonn, Bonn, Germany, 2010.
- [7] A. Damianou and N. Lawrence, *Deep gaussian processes*, Proceedings of the 16th International Conference on Artificial Intelligence and Statistics, 2013, pp. 207–215.
- [8] S. de Marchi and R. Schaback, *Stability of kernel-based interpolation*, Adv. Comput. Math. **32** (2010), 155–161.
- [9] G. Fasshauer and Q. Ye, *Reproducing kernels of generalized Sobolev spaces via a Green function approach with distributional operators*, Numerische Mathematik **119** (2011), no. 3, 585–611.
- [10] M. Gönen and E. Alpaydin, *Multiple kernel learning algorithms*, JMLR **12** (2011), 2211–2268.
- [11] Ian Goodfellow, Yoshua Bengio, and Aaron Courville, *Deep learning*, MIT Press, 2016.
- [12] G. Kimeldorf and G. Wahba, *A correspondence between Bayesian estimation on stochastic processes and smoothing by splines*, The Annals of Mathematical Statistics **41** (1970), no. 2, 495–502.
- [13] S. Mallat, *Understanding deep convolutional networks*, Phil. Trans. R. Soc. A **374** (2016), no. 2065.

- [14] H. Mhaskar, Q. Liao, and T. Poggio, *When and why are deep networks better than shallow ones?*, Proceedings of the 31st AAAI Conference on Artificial Intelligence, 2017, pp. 2343–2349.
- [15] C. Micchelli and M. Pontil, *On learning vector-valued functions*, Neural Computation **17** (2005), 177–204.
- [16] G. Montavon, S. Lapuschkin, A. Binder, W. Samek, and K.-R. Müller, *Explaining nonlinear classification decisions with deep Taylor decomposition*, Pattern Recognition **65** (2017), 211–222.
- [17] I. Rebai, Y. Benayed, and W. Mahdi, *Deep multilayer multiple kernel learning*, Neural Computing and Applications **27** (2016), no. 8, 2305–2314.
- [18] S. Reddi, S. Sra, B. Póczos, and A. Smola, *Proximal stochastic methods for nonsmooth nonconvex finite-sum optimization*, Advances in Neural Information Processing Systems 29 (D. D. Lee, M. Sugiyama, U. V. Luxburg, I. Guyon, and R. Garnett, eds.), Curran Associates, Inc., 2016, pp. 1145–1153.
- [19] B. Schölkopf and A. Smola, *Learning with Kernels – Support Vector Machines, Regularization, Optimization, and Beyond*, The MIT Press – Cambridge, Massachusetts, 2002.
- [20] E. Strobl and S. Visweswaran, *Deep multiple kernel learning*, Proceedings of the 12th International Conference on Machine Learning and Applications, 2013, pp. 414–417.
- [21] H. Wendland, *Scattered Data Approximation*, Cambridge Monographs on Applied and Computational Mathematics, Cambridge University Press, 2005.
- [22] A. Wilson, Z. Hu, R. Salakhutdinov, and E. Xing, *Deep kernel learning*, Proceedings of the 19th International Conference on Artificial Intelligence and Statistics, 2016, pp. 370–378.
- [23] J. Zhuang, I. Tsang, and S. Hoi, *Two-layer multiple kernel learning*, Proceedings of the 14th International Conference on Artificial Intelligence and Statistics, 2011, pp. 909–917.